

Heterogeneous Catalysis

Bifunctional Europium for *Operando* Catalyst Thermometry in an Exothermic Chemical Reaction

Bas J. P. Terlingen, Tjom Arens, Thomas P. van Swieten, Freddy T. Rabouw, P. Tim Prins, Michiel M. de Beer, Andries Meijerink, Mathieu P. Ahr, Eline M. Hutter, Coert E. J. van Lare, and Bert M. Weckhuysen*

Abstract: Often the reactor or the reaction medium temperature is reported in the field of heterogeneous catalysis, even though it could vary significantly from the reactive catalyst temperature. The influence of the catalyst temperature on the catalytic performance and vice versa is therefore not always accurately known. We here apply EuOCl as both solid catalyst and thermometer, allowing for *operando* temperature determination. The interplay between reaction conditions and the catalyst temperature dynamics is studied. A maximum temperature difference between the catalyst and oven of +16 °C was observed due to the exothermicity of the methane oxychlorination reaction. Heat dissipation by radiation appears dominating compared to convection in this set-up, explaining the observed uniform catalyst bed temperature. Application of *operando* catalyst thermometry could provide a deeper mechanistic understanding of catalyst performances and allow for safer process operation in chemical industries.

Temperature is arguably the most important parameter in catalysis as it dominates the reaction kinetics, thermodynamics and stability of the catalyst.^[1,2] These phenomena determine the overall feasibility of a chemical process. Almost all publications in the field consider only the

temperature of the reactor or reaction medium, thereby assuming that the catalyst bodies have the same temperature. The influence of the reaction thermodynamics and kinetics is not considered in most cases, undermining the spatiotemporal temperature changes of the catalyst bodies under reaction conditions. It is somewhat surprising that, after more than a century of heterogeneous catalysis research, very limited information is available on the local temperature of the catalyst bodies under true working conditions further emphasizing the need and importance of *operando* spectroscopy research.^[3–13]

In the handful of articles published on *operando* catalyst thermometry currently available, large discrepancies between the set reactor temperature and the catalyst temperature were reported.^[7,8] Previous research evidenced that local temperature was highly influenced by the reaction mixture fed in the reactor, inducing heat generation (+80 °C from set point)^[7] or heat removal (−65 °C from set point).^[8] These results stress the importance of monitoring the local temperature as precise control is crucial for stable, safe, and efficient catalytic conversion processes.^[14–17] *Operando* determination of the catalyst temperature is especially interesting in exothermic reactions. As a case study, we have chosen in this work the methane oxychlorination (MOC) reaction, which has to potential to see commercialization, but operating this potentially hazardous reaction is far from trivial.^[18–25] The reaction $\text{CH}_4 + \text{HCl} + \frac{1}{2}\text{O}_2 \rightarrow \text{CH}_3\text{Cl} + \text{H}_2\text{O}$ is highly exothermic, with a reaction enthalpy of $\Delta H_{773\text{K}}^0 = -157.6 \text{ kJ mol}^{-1}$, operated at >400 °C, the reaction feed/products mixtures are corrosive, potentially explosive, and toxic.^[26,27] Process safety is thus a top priority for conducting this chemical reaction.

The application of *operando* catalyst thermometry in the methane oxychlorination reaction enables real-time control over the catalyst performance and process safety. A hazardous thermal runaway can be identified in an early stage, without the temperature detection delay from which traditional temperature measurement techniques suffer.^[28–30] EuOCl is a unique catalyst for methane oxychlorination, because it is not only catalytically active, but also shows temperature-sensitive luminescence. In contrast to the method applied in literature, where typically thermometric particles are added to the catalyst, we can ensure that the temperature of the catalyst is measured.^[7,8] Furthermore, this eliminates the potential influence of the thermometric particles on the catalytic activity. Thus, this bifunctionality

[*] B. J. P. Terlingen, T. Arens, T. P. van Swieten, Dr. F. T. Rabouw, P. T. Prins, Prof. Dr. A. Meijerink, Dr. E. M. Hutter, Prof. Dr. B. M. Weckhuysen

Debye Institute for Nanomaterials Science and Institute for Sustainable and Circular Chemistry, Department of Chemistry, Utrecht University

Universiteitsweg 99, 3584 CG Utrecht (The Netherlands)
E-mail: b.m.weckhuysen@uu.nl

M. M. de Beer, Dr. C. E. J. van Lare
Nobian

Zutphenseweg 10, 7418 AJ Deventer (The Netherlands)

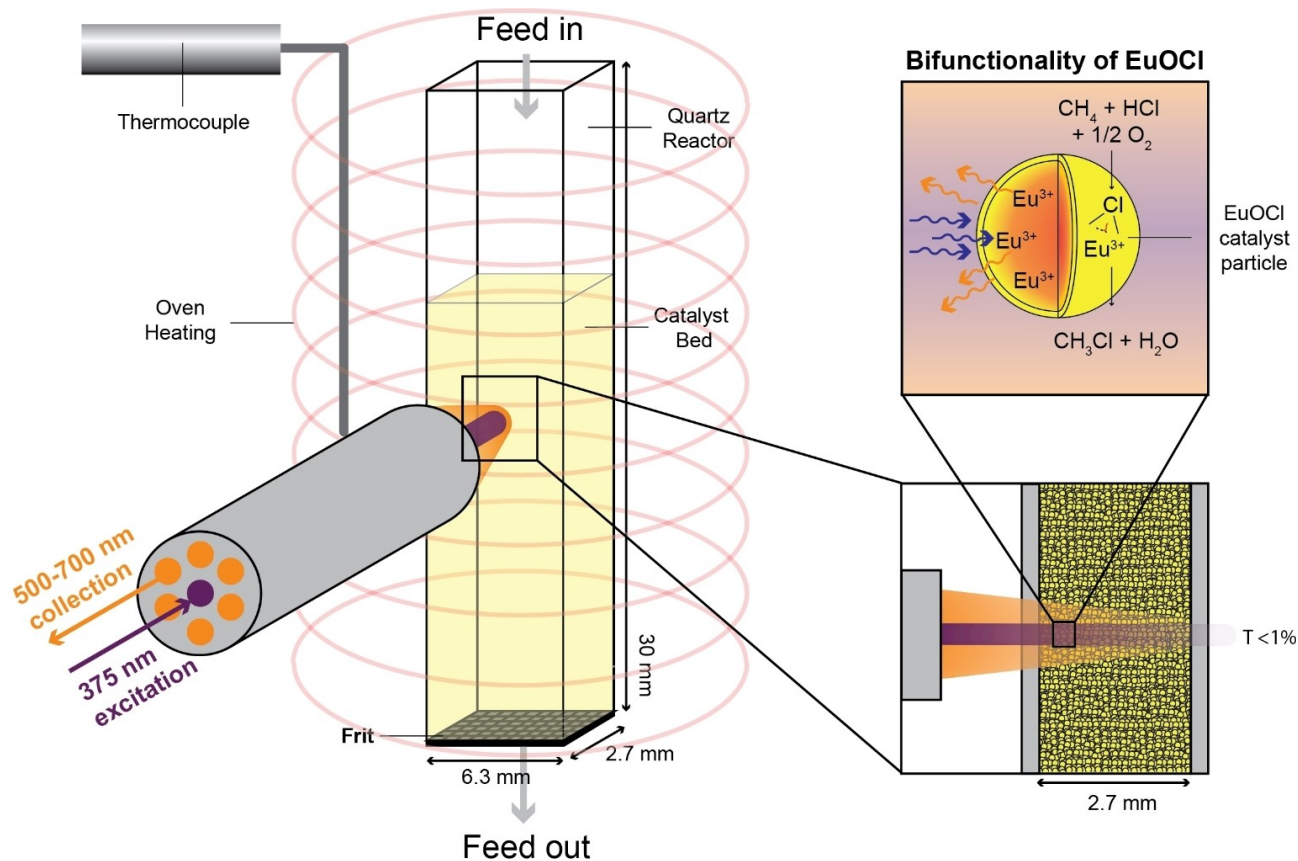
Dr. M. P. Ahr
KLK Kolb Specialties
Langestraat 137, 7491 AE Delden (The Netherlands)

© 2022 The Authors. Angewandte Chemie International Edition published by Wiley-VCH GmbH. This is an open access article under the terms of the Creative Commons Attribution License, which permits use, distribution and reproduction in any medium, provided the original work is properly cited.

enables local temperature measurements at the active catalytic site without influencing the catalysis. The bifunctionality concept and the visualization of the experimental set-up is depicted in Scheme 1. The spot size of the laser is in the millimetre range, measuring the temperature of numerous catalyst bodies (125–425 μm sieve fraction) that are agglomerates of individual EuOCl catalyst particles (< 500 nm).^[27] Hence, an average temperature of numerous catalyst particles is obtained. At the surface of an individual catalyst particle, the methane oxychlorination reaction proceeds and heat is generated due to the exothermicity of the possible reactions (see Supporting Information section 2). Under reaction conditions, Eu^{3+} is excited with a 375 nm laser, penetrating the surface of the individual catalyst particle. This generates luminescence both at the surface and in the interior part of the catalyst, enabling temperature measurements of the entire catalyst particle. UV-light typically has a penetration depth of <100 μm in strongly scattering media such as a bed of micrometre-sized particles.^[31] Hence, penetration of the laser through the catalyst bed is not expected. We confirmed this by performing absorbance and transmittance measurements (Figure S2). The absorption at 375 nm was relatively high and

less than 1% of the incident beam could pass through the EuOCl-filled quartz reactor.

The bifunctional EuOCl catalyst material was synthesized (see Supporting Information section 1 for more experimental details) in the desired EuOCl crystal phase (Figure S3A) with an irregularly shaped morphology (Figure S3B).^[25,27,32] The excitation of EuOCl with 375 nm light yielded sharp emissions (Figure S4), which could all be assigned according to the energy diagram of Eu^{3+} (Figure 1A).^[33,34] The EuOCl catalyst material showed temperature-dependent emission from 400 to 550 $^{\circ}\text{C}$ (Figure 1B). Specifically, we observe variations in the relative emission intensity from the thermally coupled $^5\text{D}_0$ and $^5\text{D}_1$ states, specifically the $^5\text{D}_1 \rightarrow ^7\text{F}_{1,2}$ and $^5\text{D}_0 \rightarrow ^7\text{F}_2$ emissions, denoted I_2 and I_1 , respectively (Figure 1C). The temperature-dependent emission was calibrated in inert conditions (20 mL min^{-1} N_2 , $1^{\circ}\text{C min}^{-1}$) and could be described according to the Boltzmann model. This yielded an energy difference between the two thermally coupled states ΔE of 1804 cm^{-1} corresponding to the expected value of 1760 cm^{-1} .^[33] Furthermore, the catalyst temperature as determined by the Boltzmann model (T_{ca}) was not influenced by the gas flow (Figure S5). We therefore assume that the temperature of



Scheme 1. Visualization of the experimental set-up, in which the bifunctionality of EuOCl as catalyst material and thermometer can be analyzed simultaneously. The quartz reactor is situated in the oven and the laser probe is aligned perpendicular to the quartz window. The 375 nm laser illuminates a part of the catalyst bed and the emission is collected through the same probe. The penetration of the incident beam through the filled quartz reactor is less than 1% at 375 nm. The thermocouple is situated in the oven on the same height as the laser. The reactive feed passes the top of the catalyst bed first, and leaves through the bottom to the gas chromatograph (GC).

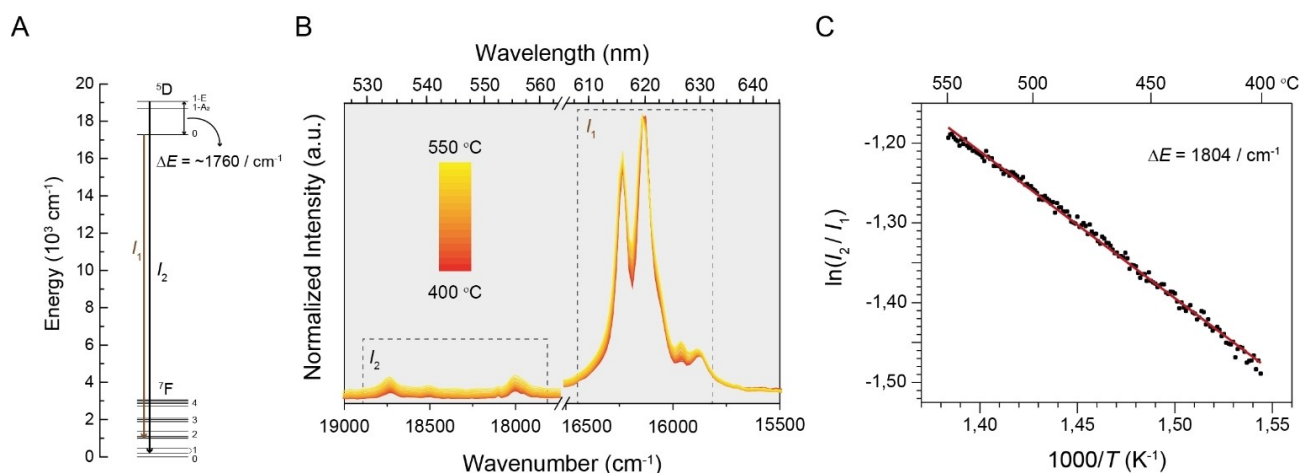


Figure 1. A) Energy diagram of Eu^{3+} where the energy gap (ΔE) between the $5D_1$ and $5D_0$ states is indicated. B) Emission spectra of EuOCl upon excitation at 375 nm from 400 (red) to 550 °C (yellow) with increments of 10 °C, where the $5D_1$ and $5D_0$ emissions are indicated by I_2 and I_1 respectively. C) The ratio of integrated emission intensities of the $5D_1$ and $5D_0$ states (see Supporting Information section 3.1, 3.2 and Figure S1 for details on data analysis) as a function of the inverse temperature. The straight line is a fit to the Boltzmann model, yielding a $5D_1$ - $5D_0$ ΔE of 1804 cm^{-1} .

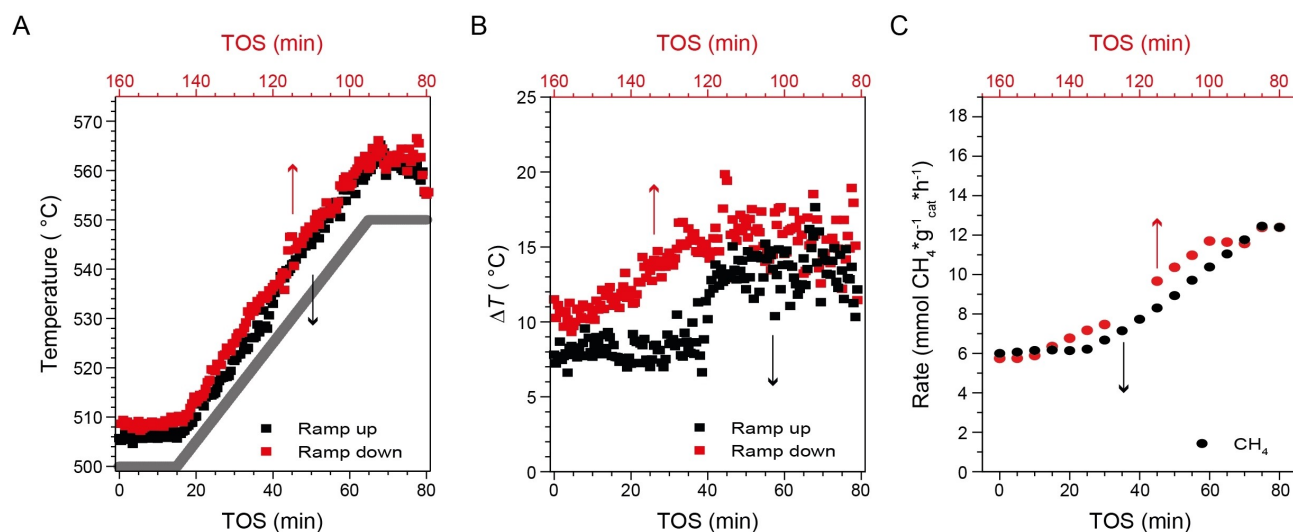


Figure 2. A) Temperature ramp-up and ramp-down between 500 °C and 550 °C where the catalyst temperature as determined by the Boltzmann model (T_{cat}) and oven temperature (T_{oven}) are plotted versus the time-on-stream (TOS). B) ΔT defined as the difference between T_{cat} and T_{oven} plotted versus TOS. C) Simultaneous to the temperature measurements, the activity was measured and the CH_4 conversion rate is given. In all cases, the black data points correspond to the bottom x-axis and the red data points correspond to the upper x-axis. Reaction conditions: CH_4 : HCl : O_2 : N_2 : He of 8:8:4:4:0 (in mL min^{-1}), $T_{\text{oven}} = 500\text{--}550 \text{ °C}$ with a ramp rate of 1 °C min^{-1} , $W_{\text{cat}} = 500 \text{ mg}$.

the feed gas is equal to T_{oven} . Bulk chlorination of EuOCl to EuCl_3 can occur under reaction conditions when the chlorination reaction occurs at a faster rate than the dechlorination reaction.^[26,27] This must be avoided as it will yield a faulty temperature read-out because of two reasons. The first reason is that the emission spectrum of EuCl_3 differs from EuOCl . Hence, if the $5D_1/5D_0$ ratio is used for the I_2/I_1 ratio, it will result in a measurement error. The second reason is that the luminescence signal of EuCl_3 is quenched at reaction temperatures, inducing a large temperature uncertainty.^[27] Since the luminescence of EuCl_3 is relatively weak, we can use the emission intensity as an

indication for the undesired formation of EuCl_3 . Indeed, we observed a loss of luminescence signal at temperatures below 500 °C under chlorinating conditions, which is likely caused by formation of EuCl_3 (Figure S6). To prevent bulk chlorination and ensure accurate temperature measurements, we will carry out the experiments at temperatures at or above 500 °C.

The catalyst temperature was significantly increased due to the heat generation under MOC reaction conditions (Figure 2). A temperature ramp-up and ramp-down between 500 °C and 550 °C revealed a significant discrepancy between the T_{oven} and T_{cat} , further denoted as ΔT , where catalyst

heating was observed over the entire temperature range (Figure 2A). At $T_{\text{oven}}=500^{\circ}\text{C}$ (0–15 min), a ΔT of 8°C was observed, which increased to 13°C at $T_{\text{oven}}=550^{\circ}\text{C}$ (65 min, Figure 2B). When the temperature was kept at 550°C , the ΔT increased further to $\approx 16^{\circ}\text{C}$. Once T_{oven} was ramped down from 550°C to 500°C (95–145 min), the ΔT gradually decreased from 16 to 10°C . The ΔT showed a positive correlation with the observed activity in the reaction (Figure 2C). Interestingly, an asymmetry in the ΔT between the ramp up and ramp down was observed. The ΔT was higher at the same T_{oven} during the ramp down compared to the ramp up, coinciding with the higher observed activity at the same T_{oven} (Figure 2C). As a constant gas hourly space velocity (GHSV) was used, the change in ΔT can be ascribed to the positive feedback between reaction rate and local temperature.

To shed light on the interplay between catalyst cooling and heat generation, three different variations in the feed composition were investigated. The response on the activity and local temperature was analyzed. Increasing the GHSV while keeping the feed composition unaltered resulted in an increase in the ΔT (Figure 3A). The increase in ΔT can be explained by the increase in reaction rate of both O_2 and CH_4 . The higher flow of reactive gas generated more reaction heat than was removed by the higher gas flow rate. The opposite effect was observed when the feed was diluted with inert He (Figure 3B). The increasing GHSV lowered the ΔT while also decreasing the reaction rate of O_2 and CH_4 . Note that at low reaction rates, the ΔT was roughly 0°C . Finally, the GHSV was kept constant while the activity was increased (Figure 3C). This was achieved by varying the HCl:He ratio while keeping a constant total flow.^[27] Again, the reaction rate of CH_4 and O_2 were positively correlated to the ΔT . Here, the change in ΔT is purely a kinetic effect as the cooling rate by convection can be regarded constant.

Both under varying oven temperatures (Figure 2) as well as under varying reaction gas feed compositions (Figure 3), the reaction rate was positively correlated to the ΔT . Furthermore, an increase in the GHSV did not always result in enhanced heat removal, as the reaction rate was not correlated to the GHSV. Heat transfer calculations (Supporting Information section 3.3) evidenced that heat loss due to convection is negligible compared to radiation. Any heat generated by the reaction will quickly dissipate by radiation until an equilibrium temperature is reached. Hence, a uniform catalyst temperature over the length of the bed is expected. Our qualitative approach was able to explain the observed trends, but we were unable to describe the change in temperature quantitatively. To verify the uniformity of the catalyst bed temperature, the T_{cat} was determined at the top and bottom of the catalyst bed (Figure 4) under MOC conditions where the GHSV was varied. As the experimental set-up did not allow for simultaneous temperature determination of the catalyst at the top and bottom of the bed, the temperatures were determined in a sequential manner. First the top of the catalyst was probed and subsequently the bed height with respect to the probe was altered to enable the temperature determination of the bottom part. A constant reaction rate

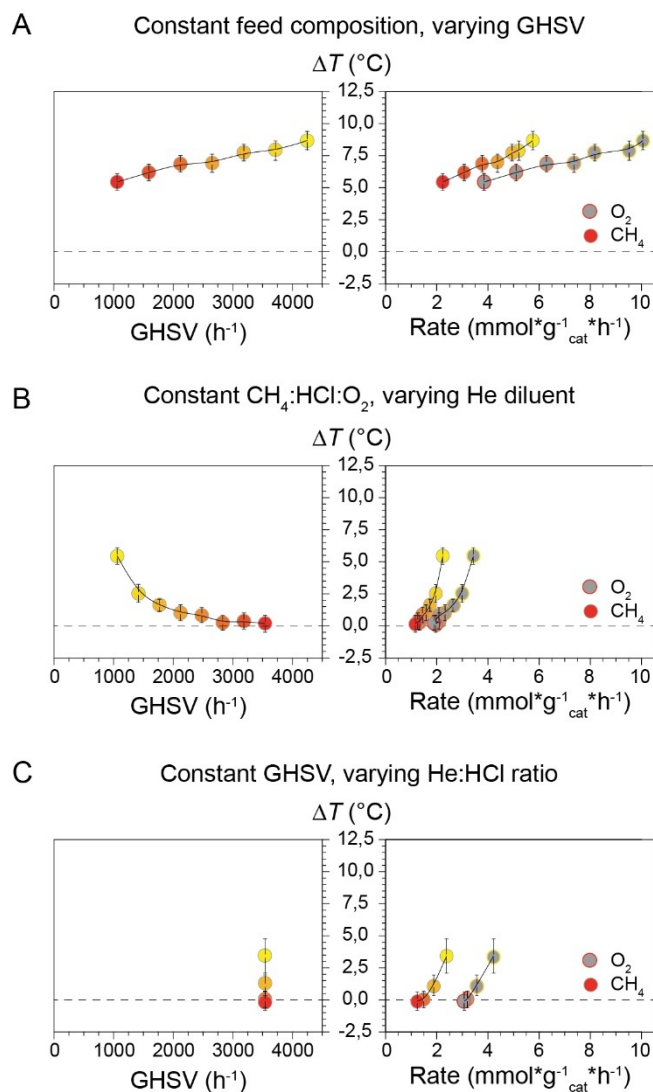


Figure 3. Temperature difference between the T_{oven} and T_{cat} , defined as ΔT , plotted versus the variable parameter gas hourly space velocity (GHSV, left window) and the resulting reaction rate for CH_4 and O_2 (right window). A) The total flow was increased without altering the gas feed composition ($\text{CH}_4:\text{HCl}:\text{O}_2:\text{N}_2:\text{He}$ 2:2:1:1:0). B) The reaction mixture was diluted with inert He ($\text{CH}_4:\text{HCl}:\text{O}_2:\text{N}_2:\text{He}$ 2:2:1:1: x (in mL min^{-1}) where $x=0-14$ with increments of 2). C) The HCl:He ratio in the feed was altered while maintaining the same total flow ($\text{CH}_4:\text{HCl}:\text{O}_2:\text{N}_2:\text{He}$ 2:16- x :1:1: x (in mL min^{-1}) where $x=0$ (yellow), 4 (orange), 8 (dark orange), 14 (red)). See Figure S7 for more information. Reaction conditions: $T_{\text{oven}}=500^{\circ}\text{C}$, $W_{\text{cat}}=500$ mg, $V_{\text{cat}}=0.34$ cm^3 .

confirmed that the catalyst activity was the same in subsequent experiments. Furthermore, the bottom part of the catalyst bed was roughly as active as the top part, since a decrease in the catalyst loading by half resulted in a reduction of the X_{CH_4} by the same amount (Figure S8). Overall, we observed no significant difference in temperature between the top and the bottom of the reactor, consistent with radiation as the dominant heat dissipation mechanism.

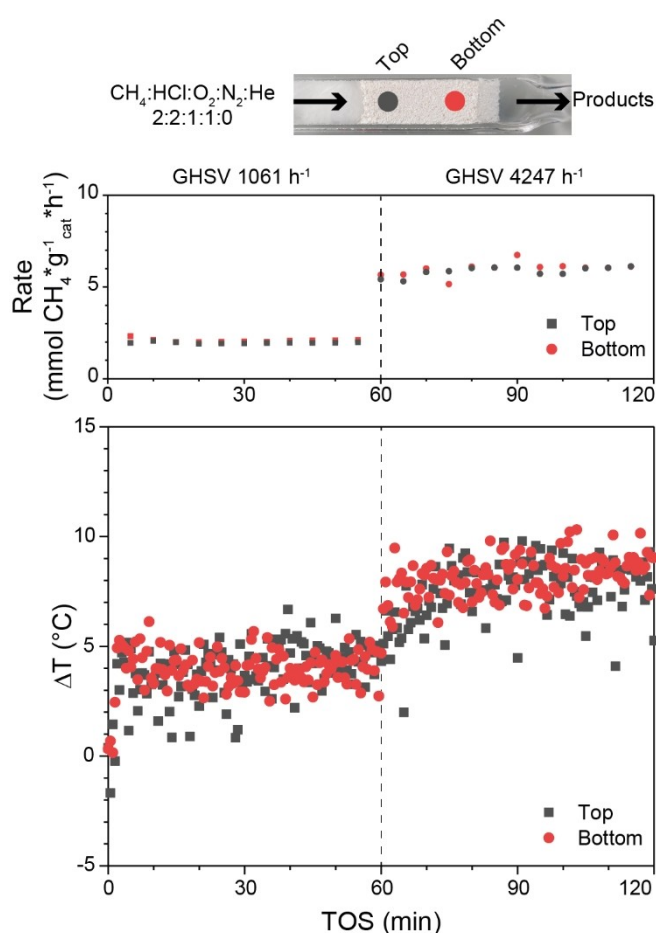


Figure 4. The reaction rate and the temperature difference between the T_{oven} and T_{cat} , defined as ΔT , plotted versus the time-on-stream (TOS). Catalyst temperature was determined at different bed heights, separated 9 mm apart. After a stabilization period of 30 min under N_2 , the reaction mixture was introduced. The temperature of the top part and bottom part were measured sequentially. Reaction conditions: $CH_4:HCl:O_2:N_2:He$ of 2:2:1:1:0 (total flow 6 or 24 $mL\ min^{-1}$), $T_{\text{oven}} = 500^\circ C$, $W_{\text{cat}} = 500\ mg$, $V_{\text{cat}} = 0.34\ cm^3$.

The bifunctionality of $EuOCl$, i.e., the catalytic activity in the MOC reaction and its temperature-dependent luminescence, enabled the rapid, stable, and direct temperature determination of catalyst particles under reaction conditions. The apparent heat balance between heat generation and heat loss was investigated by varying the feed composition and the reaction temperature. Under various conditions we observed a higher catalyst temperature compared to the oven set temperature. This temperature difference ΔT correlated strongly to the reaction rate. The maximum ΔT observed was $16^\circ C$. Heat-balance calculations were able to describe the observed trends qualitatively and identified radiation as the dominant heat dissipation mechanism. This was consistent with the measured uniform catalyst bed temperature. To be able to describe the temperature increase quantitatively, a more detailed model must be constructed and more carefully controlled experiments must be conducted, which will form the basis of a follow-up study. We anticipate that the concept of *operando* thermometry in

chemical reactions can be transferred to other fields where lanthanide-based catalysts are used. These fields include reactions where a lanthanide acts as catalytic center, e.g. reactions involving halogens,^[35–40] or promotor, e.g. reforming reactions^[41,42] and methanol synthesis^[43] in which La^{3+} would be (partially) substituted by Eu^{3+} . Lastly, the application of thermometric support materials^[44–47] opens up the possibility to perform *operando* thermometry in chemical reactions where lanthanides typically do not play a role. Hence, the integrated functional material-thermometer concept, successfully explored in this work of the MOC reaction, can be extended to a wide variety of processes and materials.

Acknowledgements

This work is part of the Advanced Research Center Chemical Building Blocks (ARC CBBC), which is co-founded and co-financed by the Netherlands Organisation for Scientific Research (NWO) and the Netherlands Ministry of Economic Affairs and Climate Policy. Furthermore, the authors would like to thank Bart Zwijnenburg (Nobian) for helping with finalizing the manuscript.

Conflict of Interest

The authors declare no conflict of interest.

Data Availability Statement

The data that support the findings of this study are available from the corresponding author upon reasonable request.

Keywords: Europium · Heterogeneous Catalysis · Methane · *Operando* Methods · Thermometry

- [1] G. Ertl, H. Knözinger, J. Weitkamp, F. Schuth, *Handbook of Heterogeneous Catalysis*, 2nd ed., Wiley-VCH, Weinheim, **2008**.
- [2] G. A. Somorjai, Y. Li, *Introduction to Surface Chemistry and Catalysis*, 1st ed., Wiley, Hoboken, **2010**.
- [3] C. Krishnaraj, H. Rijckaert, H. S. Jena, P. Van Der Voort, A. M. Kaczmarek, *ACS Appl. Mater. Interfaces* **2021**, *13*, 47010–47018.
- [4] A. M. Kaczmarek, H. S. Jena, C. Krishnaraj, H. Rijckaert, S. K. P. Veerapandian, A. Meijerink, P. Van Der Voort, *Angew. Chem. Int. Ed.* **2021**, *60*, 3727–3736; *Angew. Chem.* **2021**, *133*, 3771–3780.
- [5] T. Park, Y.-J. Guan, Z.-Q. Liu, Y. Zhang, *Phys. Rev. Appl.* **2018**, *10*, 034049.
- [6] H. S. Jena, H. Rijckaert, C. Krishnaraj, I. Van Driessche, P. Van Der Voort, A. M. Kaczmarek, *Chem. Mater.* **2021**, *33*, 8007–8017.
- [7] R. G. Geitenbeek, A.-E. Nieuwelink, T. S. Jacobs, B. B. V. Salzmann, J. Goetze, A. Meijerink, B. M. Weckhuysen, *ACS Catal.* **2018**, *8*, 2397–2401.
- [8] T. Hartman, R. G. Geitenbeek, G. T. Whiting, B. M. Weckhuysen, *Nat. Catal.* **2019**, *2*, 986–996.

- [9] I. K. van Ravenhorst, R. G. Geitenbeek, M. J. van der Eerden, J. Tijn van Omme, H. H. Peréz Garza, F. Meirer, A. Meijerink, B. M. Weckhuysen, *ChemCatChem* **2019**, *11*, 5505–5512.
- [10] B. Dong, D. P. Liu, X. J. Wang, T. Yang, S. M. Miao, C. R. Li, *Appl. Phys. Lett.* **2007**, *90*, 181117.
- [11] P. P. Lima, F. A. A. Paz, C. D. S. Brites, W. G. Quirino, C. Legnani, M. Costa, E. Silva, R. A. S. Ferreira, S. A. Júnior, O. L. Malta, M. Cremona, L. D. Carlos, *Org. Electron.* **2014**, *15*, 798–808.
- [12] H. Suo, F. Hu, X. Zhao, Z. Zhang, T. Li, C. Duan, M. Yin, C. Guo, *J. Mater. Chem. C* **2017**, *5*, 1501–1507.
- [13] B. Hou, M. Jia, P. Li, G. Liu, Z. Sun, Z. Fu, *Inorg. Chem.* **2019**, *58*, 7939–7946.
- [14] N. E. Tsakoumis, M. Rønning, Ø. Borg, E. Rytter, A. Holmen, *Catal. Today* **2010**, *154*, 162–182.
- [15] R. Gygax, *Chem. Eng. Sci.* **1988**, *43*, 1759–1771.
- [16] J. Werther, *Powder Technol.* **1999**, *102*, 15–36.
- [17] D. Moodley, M. Claeys, E. van Steen, P. van Helden, D. Kistamurthy, K. J. Weststrate, H. Niemantsverdriet, A. Saib, W. Erasmus, J. van de Loosdrecht, *Catal. Today* **2020**, *342*, 59–70.
- [18] L. Sun, Y. Wang, N. Guan, L. Li, *Energy Technol.* **2020**, *8*, 1900826.
- [19] A. I. Olivios-Suarez, À. Szécsényi, E. J. M. Hensen, J. Ruiz-Martinez, E. A. Pidko, J. Gascon, *ACS Catal.* **2016**, *6*, 2965–2981.
- [20] M. Scharfe, G. Zichittella, V. Paunović, J. Pérez-Ramírez, *Chin. J. Catal.* **2020**, *41*, 915–927.
- [21] V. Paunović, G. Zichittella, P. Hemberger, A. Bodi, J. Pérez-Ramírez, *ACS Catal.* **2019**, *9*, 1710–1725.
- [22] G. Zichittella, N. Aellen, V. Paunović, A. P. Amrute, J. Pérez-Ramírez, *Angew. Chem. Int. Ed.* **2017**, *56*, 13670–13674; *Angew. Chem.* **2017**, *129*, 13858–13862.
- [23] G. Zichittella, V. Paunović, A. P. Amrute, J. Pérez-Ramírez, *ACS Catal.* **2017**, *7*, 1805–1817.
- [24] J. He, T. Xu, Z. Wang, Q. Zhang, W. Deng, Y. Wang, *Angew. Chem. Int. Ed.* **2012**, *51*, 2438–2442; *Angew. Chem.* **2012**, *124*, 2488–2492.
- [25] E. Peringer, S. G. Podkolzin, M. E. Jones, R. Olindo, J. A. Lercher, *Top. Catal.* **2006**, *38*, 211–220.
- [26] B. Terlingen, R. Oord, M. Ahr, E. M. Hutter, C. Van Lare, B. M. Weckhuysen, *ACS Catal.* **2022**, *12*, 5698–5710.
- [27] B. Terlingen, R. Oord, M. Ahr, E. Hutter, C. Van Lare, B. M. Weckhuysen, *ACS Catal.* **2021**, *11*, 10574–10588.
- [28] A. Kummer, T. Varga, *Process Saf. Environ. Prot.* **2021**, *147*, 460–476.
- [29] J. Juncheng, W. Dan, N. Lei, F. Gang, P. Yong, *J. Loss Prev. Process Ind.* **2020**, *64*, 104093.
- [30] B. Liu, Q. Huang, P. Wang, *Case Stud. Therm. Eng.* **2020**, *19*, 100627.
- [31] D. Oelkrug, M. Brun, K. Rebner, B. Boldrini, R. Kessler, *Appl. Spectrosc.* **2012**, *66*, 934–943.
- [32] E. Peringer, M. Salzinger, M. Hutt, A. A. Lemonidou, J. A. Lercher, *Top. Catal.* **2009**, *52*, 1220–1231.
- [33] L. G. Deshazer, G. H. Dieke, *J. Chem. Phys.* **1963**, *38*, 2190–2199.
- [34] J. Hölsä, P. Porcher, *J. Chem. Phys.* **1981**, *75*, 2108–2117.
- [35] M. Scharfe, P. A. Lira-Parada, A. P. Amrute, S. Mitchell, J. Pérez-Ramírez, *J. Catal.* **2016**, *344*, 524–534.
- [36] H. Ma, Y. Wang, Y. Qi, K. R. Rout, D. Chen, *ACS Catal.* **2020**, *10*, 9299–9319.
- [37] G. Zichittella, Y. Polyhach, R. Tschaggelar, G. Jeschke, J. Pérez-Ramírez, *Angew. Chem. Int. Ed.* **2021**, *60*, 3596–3602; *Angew. Chem.* **2021**, *133*, 3640–3646.
- [38] V. Paunović, R. Lin, M. Scharfe, A. P. Amrute, S. Mitchell, R. Hauert, J. Pérez-Ramírez, *Angew. Chem. Int. Ed.* **2017**, *56*, 9791–9795; *Angew. Chem.* **2017**, *129*, 9923–9927.
- [39] B. de Rivas, N. Guillén-Hurtado, R. López-Fonseca, F. Coloma-Pascual, A. García-García, J. I. Gutiérrez-Ortiz, A. Bueno-López, *Appl. Catal. B* **2012**, *121–122*, 162–170.
- [40] A. W. A. M. Van Der Heijden, V. Bellière, L. E. Alonso, M. Daturi, O. V. Manoilova, B. M. Weckhuysen, *J. Phys. Chem. B* **2005**, *109*, 23993–24001.
- [41] A. Haryanto, S. Fernando, N. Murali, S. Adhikari, *Energy Fuels* **2005**, *19*, 2098–2106.
- [42] N. D. Charisiou, G. Siakavelas, K. N. Papageridis, A. Baklavari, L. Tzounis, D. G. Avraam, M. A. Goula, *J. Nat. Gas Sci. Eng.* **2016**, *31*, 164–183.
- [43] H. Ban, C. Li, K. Asami, K. Fujimoto, *Catal. Commun.* **2014**, *54*, 50–54.
- [44] G. Hirata, N. Perea, M. Tejada, J. A. Gonzalez-Ortega, J. McKittrick, *Opt. Mater.* **2005**, *27*, 1311–1315.
- [45] R. G. Geitenbeek, P. T. Prins, W. Albrecht, A. Van Blaaderen, B. M. Weckhuysen, A. Meijerink, *J. Phys. Chem. C* **2017**, *121*, 3503–3510.
- [46] T. Myint, R. Gunawidjaja, H. Eilers, *J. Phys. Chem. C* **2012**, *116*, 21629–21634.
- [47] R. G. Geitenbeek, B. B. V. Salzmänn, A.-E. Nieuwelink, A. Meijerink, B. M. Weckhuysen, *Chem. Eng. Sci.* **2019**, *198*, 235–240.

Manuscript received: August 13, 2022

Accepted manuscript online: November 3, 2022

Version of record online: November 24, 2022